Title

Optimization of Corner Blending Curves

Authors

Farouki, RT
Pelosi, F
Sampoli, ML

Publication Date

2019-12-01

DOI

10.1016/j.cad.2019.102739

Peer reviewed

Optimization of corner blending curves

Rida T. Farouki
Department of Mechanical and Aerospace Engineering,
University of California, Davis, CA 95616, USA.
Francesca Pelosi
Dipartimento di Matematica, Università di Roma "Tor Vergata,"
Via della Ricerca Scientifica, 00133 Roma, Italy.
Maria Lucia Sampoli
Dipartimento di Ingegneria dell'Informazione e
Scienze Matematiche, Università di Siena, San Niccolò,
Via Roma 56, 53100 Siena, Italy.

Abstract

The blending or filleting of sharp corners is a common requirement in geometric design applications — motivated by aesthetic, ergonomic, kinematic, or mechanical stress considerations. Corner blending curves are usually required to exhibit a specified order of geometric continuity with the segments they connect, and to satisfy specific constraints on their curvature profiles and the extremum deviation from the original corner. The free parameters of polynomial corner curves of degree ≤ 6 and continuity up to G^3 are exploited to solve a convex optimization problem, that minimizes a weighted sum of dimensionless measures of the mid–point curvature, maximum deviation, and the uniformity of parametric speed. It is found that large mid–point curvature weights result in undesirable bimodal curvature profiles, but emphasizing the parametric speed uniformity typically yields favorable outcomes (since the curvature is strongly dependent upon parametric speed variation). A constrained optimization problem, wherein a particular value of the corner curve deviation is specified, is also addressed. Finally, the shape of Pythagorean–hodograph corner curves is compared with that of the optimized "ordinary" polynomial corner curves.

Keywords: corner blending curves; geometric continuity; shape optimization; curvature distribution; parametric speed; Pythagorean–hodograph curves.

e–mail: farouki@ucdavis.edu, pelosi@mat.uniroma2.it, marialucia.sampoli@unisi.it

1 Introduction

In many design contexts, smooth blends between extended "simple" (linear or circular) segments are required. Typically, these blending curves are required to exhibit a prescribed order of geometric continuity with the segments they connect, and to have well–behaved (e.g., monotone or unimodal) curvature profiles. In consumer products design, for example, rounded corners are often preferred to satisfy aesthetic or ergonomic considerations, and in the design of load–bearing mechanical components, the rounding or "filleting" of sharp corners is essential in minimizing stress concentration and thereby enhancing fatigue life. In CNC machining, sharp corners in piecewise–linear toolpaths must be rounded to permit accurate high–speed execution without incurring excessive decelerations and accelerations [2, 8, 18, 19, 21, 25, 26, 27, 28, 29]. An analogous concern occurs in the layout of highways or railways, wherein precise control of the curvature of transition curves is required to guarantee compatibility with prescribed safe vehicle traversal speeds [1, 17, 23, 24].

For blend curves that connect segments of disparate curvature (e.g., linear and circular segments, or two circle segments with different radii), monotone curvature variation is preferred, and such "spiral" blend segments have been extensively studied [4, 7, 13, 14, 15, 16, 20, 30, 31, 32, 33, 34, 35, 37]. For blend curves connecting two linear segments, however, a symmetric unimodal curvature profile that yields the desired change of direction (or *turning angle*) is desired [6, 36]. The focus of the present study is on the latter context, and in particular on the formulation and optimization of an appropriate measure of the overall quality of corner blending curves.

A number of key features of corner blending curves may be identified:

(1) they should exhibit symmetry about their mid–points, and a prescribed order of geometric continuity G^k with the linear segments they connect;

(2) they should be free of inflections and have unimodal curvature profiles;

(3) they should represent a reasonable compromise between minimizing the mid–point curvature κ_{m} and deviation δ_{m} from the sharp corner.

These considerations often exert conflicting influences in the design of corner curves. For a symmetric unimodal curvature profile, the maximum curvature κ_{m} occurs at the mid point. However, for a given corner geometry, too much emphasis on minimizing the mid–point curvature (for aesthetic or kinematic purposes) can incur an unacceptably large deviation δ_{m} or bimodal curvature distribution. Finally, most applications demand at least G^1 (more often G^2) continuity. However, for G^3 or higher orders of continuity, the corner curve can possess extended regions of low curvature at the end points, and a sharp spike in curvature about the mid point. Thus, the purpose of the optimization process is to seek a "balance" among these conflicting influences.

1.1 Contributions of this study

The intent of this paper is to formulate and demonstrate algorithms for the shape optimization of corner curves, based on the criteria enumerated above. The algorithms are designed to provide flexibility regarding emphasis on the design criteria (e.g., minimization of κ_{m} versus minimization of δ_{m}), to suit different applications. However, the focus here is on the fundamental corner curve intrinsic geometry, rather than specific applications. The criteria stated above are not exhaustive, and the basic metholodogy presented herein can be adapted on an as–needed basis, to satisfy particular technical constraints — e.g., by imposing a bound on concave curvatures, for gouge–free machining with a tool of given radius; or using variable feedrates along corner curves, to manage axis accelerations in CNC machining or 3D printing.

1.2 Organization of the paper

The remainder of this paper is organized as follows. Section 2 introduces the "canonical form" of the corner rounding problem, which serves to simplify the analysis, and discusses key features of the corner curves. The properties of polynomial corner curves of degrees up to $n = 6$ and continuity class up to G^3 are then presented in Section 3, while Section 4 addresses the formulation of dimensionless objective functions, based upon the mid–point curvature and deviation, and uniformity of parameterization of corner blending curves, that can be used to optimize them with respect to the available free parameters. Section 5 summarizes the numerical optimization schemes used to determine the minima of these objective functions, and Section 6 presents a number of examples to illustrate the optimal corner curves obtained for various choices of the weights. In Section 7, Pythagorean–hodograph (PH) corner blending curves are compared with optimized "ordinary" polynomial curves for a given order of geometric continuity. Since they possess fewer shape freedoms, for a given turning angle θ, there are unique G^1, G^2, G^3 PH corner curves of degree $3, 5, 7$. The G^1 PH corners are similar to the optimized ordinary cubics, but G^2 and G^3 PH corner curves have smaller deviations δ_{m} and larger curvatures κ_{m} than analogous optimized ordinary polynomial curves. Finally, the main results of the present study are summarized in Section 8, and some issues that deserve further investigation are identified.

2 Canonical corner blending problem

The rounding of sharp corners in piecewise–linear loci has been considered by many authors, most frequently in the context of ensuring smoother execution of G code part programs in CNC machining [2, 6, 8, 21, 27, 28, 29, 36]. The

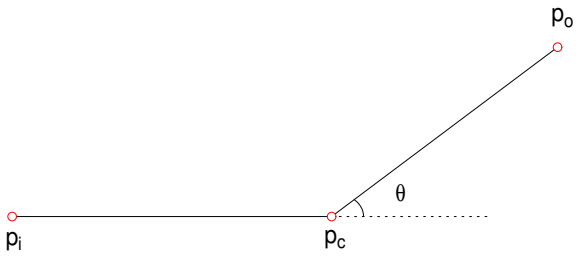

Figure 1: Canonical data for a corner blending curve.

emphasis in these studies is mainly on ensuring smooth (G^1 or preferably G^2) junctures of corner curves with the linear segments they connect, to preclude velocity or acceleration discontinuities. A numerical method to minimize the extremum curvature of a G^2 quintic Bézier corner curve was proposed in [25]. Building on prior work, the present study proposes a systematic approach to exploiting the residual free parameters of corner curves (for a specified order of geometric continuity) to minimize a combination of extremum curvature, corner deviation, and parametric speed variation. By different weightings of these terms, the objective function can be tailored to particular applications, and it can also be generalized by appending constraint equalities/inequalities, or introducing additional terms in the optimization objective function.

Consider the rounding of two linear segments that meet at a corner point $\mathbf{p}_c$. The sharp corner is to be "rounded" by a smooth curve $\mathbf{r}(\xi)$, $\xi \in [\,0,1\,]$ that begins at a point $\mathbf{p}_i$ on the incoming line segment, and ends at a point $\mathbf{p}_o$ on the outgoing line segment, i.e., $\mathbf{r}(0) = \mathbf{p}_i$ and $\mathbf{r}(1) = \mathbf{p}_o$, and to ensure a symmetric solution we require that $\|\mathbf{p}_c - \mathbf{p}_i\| = \|\mathbf{p}_o - \mathbf{p}_c\|$ (see Figure 1). For brevity, we consider this problem using "canonical" data with

$$\mathbf{p}_i = (-1,0)\,, \quad \mathbf{p}_c = (0,0)\,, \quad \mathbf{p}_o = (\cos\theta, \sin\theta)\,, \tag{1}$$

where θ is the corner turning angle as shown in Figure 1. The curve must have at least G^1 continuity with the line segments, i.e., it must have end tangents $\mathbf{t}(0) = \mathbf{r}'(0)/\|\mathbf{r}'(0)\| = (1,0)$ and $\mathbf{t}(1) = \mathbf{r}'(1)/\|\mathbf{r}'(1)\| = (\cos\theta, \sin\theta)$. By a suitable translation, rotation, and scaling, the corner curve $\mathbf{r}(\xi)$ can be used to smoothly blend any sharp corner in a piecewise–linear locus.

The parametric speed of the curve $\mathbf{r}(\xi) = (x(\xi), y(\xi))$ is defined by

$$\sigma(\xi) \;=\; \|\mathbf{r}'(\xi)\| \;=\; \sqrt{x'^2(\xi) + y'^2(\xi)} \;=\; \frac{\mathrm{d}s}{\mathrm{d}\xi}\,, \tag{2}$$

where s is arc length along $\mathbf{r}(\xi)$. The curvature and its arc–length derivative [9] are

$$\kappa \;=\; \frac{(\mathbf{r}' \times \mathbf{r}'') \cdot \mathbf{z}}{\sigma^3}\,, \quad \frac{\mathrm{d}\kappa}{\mathrm{d}s} \;=\; \frac{(\mathbf{r}' \times \mathbf{r}''') \cdot \mathbf{z} - 3\,\sigma^2\sigma'\kappa}{\sigma^4}\,, \tag{3}$$

where $\mathbf{z}$ is a unit vector orthogonal to the (x, y) plane. Note here that κ and $\mathrm{d}\kappa/\mathrm{d}s$ are intrinsic shape properties of the curve $\mathbf{r}(\xi)$, specified as functions of the curve parameter ξ. The derivatives of the parametric speed may be expressed as

$$\sigma' \;=\; \frac{\mathbf{r}' \cdot \mathbf{r}''}{\sigma}\,, \quad \sigma'' \;=\; \frac{\mathbf{r}' \cdot \mathbf{r}''' + \|\mathbf{r}''\|^2 - \sigma'^2}{\sigma}\,.$$

In the context of applications, two features of the corner rounding curve are of particular interest — the deviation δ_{m} of the mid–point from the original exact corner $(0, 0)$ and the mid–point curvature magnitude, namely

$$\delta_{\mathrm{m}} \;=\; \|\, \mathbf{r}(\tfrac{1}{2}) \,\| \quad \text{and} \quad \kappa_{\mathrm{m}} \;=\; |\, \kappa(\tfrac{1}{2}) \,|\,. \tag{4}$$

As two "extreme" solutions to the corner rounding problem, we note that the original corner (i.e., the piecewise–linear path from $\mathbf{p}_i$ to $\mathbf{p}_c$ to $\mathbf{p}_o$) has $\delta_{\mathrm{m}} = 0$ and $\kappa_{\mathrm{m}} = \infty$ (i.e., an impulse in curvature at $\mathbf{p}_c$), while the short–cut linear path from $\mathbf{p}_i$ to $\mathbf{p}_o$ has $\kappa_{\mathrm{m}} = 0$ and $\delta_{\mathrm{m}} = |\sin\frac{1}{2}\theta\,|$. The goal is thus to identify smooth curves, satisfying prescribed continuity conditions at $\mathbf{p}_i$ and $\mathbf{p}_o$, that balance the desire to subdue both δ_{m} and κ_{m}.

3 Polynomial corner curves

Consider the use of a planar degree n Bézier curve

$$\mathbf{r}(\xi) \;=\; \sum_{k=0}^{n} \mathbf{p}_k\, b_k^n(\xi)\,, \quad b_k^n(\xi) \;=\; \binom{n}{k}(1-\xi)^{n-k}\xi^k\,, \tag{5}$$

symmetric about the normal line at the mid–point $\mathbf{r}(\frac{1}{2})$, to define a corner curve. For even n, there is an odd number of control points, and we set

$$\mathbf{p}_0 \;=\; \mathbf{p}_i\,, \quad \mathbf{p}_{n/2} \;=\; \mathbf{p}_c\,, \quad \mathbf{p}_n \;=\; \mathbf{p}_o\,, \tag{6}$$

with the remaining control points $\mathbf{p}_k$ for $0 < k < n/2$ and $n/2 < k < n$ to be determined. For odd n, we again set $\mathbf{p}_0 = \mathbf{p}_i$ and $\mathbf{p}_n = \mathbf{p}_o$, but since the number of control points is even, it is not possible to symmetrically assign them so that one control point coincides with $\mathbf{p}_c$.

3.1 The case $n = 2$

The control points (6) achieve a G^1 connection with incoming and outcoming linear segments at angles 0 and θ relative to the x–axis, with minimum degree $n = 2$ (i.e., a parabola segment). For the case $n = 2$, we have

$$\mathbf{p}_0 \;=\; (-1, 0)\,, \quad \mathbf{p}_1 \;=\; (0, 0)\,, \quad \mathbf{p}_2 \;=\; (\cos\theta, \sin\theta)\,,$$

and the corner curve is unique (there are no free parameters). Its parametric speed and curvature are

$$\sigma(\xi) \;=\; 2\,\sqrt{(1-\xi)^2 + \cos\theta\, 2(1-\xi)\xi + \xi^2}\,, \quad \kappa(\xi) \;=\; \frac{4\,\sin\theta}{\sigma^3(\xi)}\,,$$

and the quantities (4) reduce to

$$\delta_{\rm m} \;=\; \tfrac{1}{2}\,|\,\sin\tfrac{1}{2}\theta\,|\,, \quad \kappa_{\rm m} \;=\; \frac{\sqrt{2}\,|\,\sin\theta\,|}{(1+\cos\theta)^{3/2}}\,.$$

For a given turning angle θ, this case offers no control over the quantities (4).

3.2 The case $n = 3$

In the case $n = 3$, a G^1 connection is achieved by control points of the form

$$\mathbf{p}_0 \;=\; (-1,0)\,,\;\; \mathbf{p}_1 \;=\; \lambda(-1,0)\,,\;\; \mathbf{p}_2 \;=\; \lambda(\cos\theta,\sin\theta)\,,\;\; \mathbf{p}_3 \;=\; (\cos\theta,\sin\theta)\,,$$

with $\lambda \in [\,0,1\,]$ a free parameter. For the cubic corner curve, the parametric speed and curvature are

$$\sigma(\xi) \;=\; \sqrt{f(\xi)}\,, \quad \kappa(\xi) \;=\; \frac{g(\xi)}{\sigma^3(\xi)} \tag{7}$$

where $f(\xi)$ is the quartic polynomial defined by the Bernstein coefficients

$$f_0 = f_4 = 9\,(1-\lambda)^2\,, \quad f_1 = f_3 = 9\,(1+\cos\theta)(1-\lambda)\lambda\,,$$
$$f_2 = 3\,\cos\theta\,(1-\lambda)^2 + 12\,(1+\cos\theta)\,\lambda^2\,,$$

and $g(\xi)$ is the quadratic polynomial

$$g(\xi) \;=\; 18\,\sin\theta\,(1-\lambda)\,[\,\lambda\,(1-\xi)^2 + \tfrac{1}{2}(1-\lambda)\,2(1-\xi)\xi + \lambda\,\xi^2\,]\,.$$

The quantities (4) reduce to

$$\delta_{\rm m} \;=\; \frac{|\,\sin\frac{1}{2}\theta\,|}{4}\,(3\,\lambda+1)\,, \quad \kappa_{\rm m} \;=\; \frac{8\sqrt{2}\,|\,\sin\theta\,|}{3\,(1+\cos\theta)^{3/2}}\,\frac{1-\lambda}{(1+\lambda)^2}\,. \tag{8}$$

Note that $\delta_{\rm m}$ is monotone–increasing with λ, having its minimum value when $\lambda = 0$ with $\mathbf{p}_1 = \mathbf{p}_2 = (0,0)$. On the other hand, $\kappa_{\rm m}$ is monotone–decreasing with λ, having its minimum value when $\lambda = 1$ with $\mathbf{p}_0 = \mathbf{p}_1 = (-1,0)$ and $\mathbf{p}_2 = \mathbf{p}_3 = (\cos\theta,\sin\theta)$. Figure 2 shows examples of these degree 3 corner curves for the turning angle $\theta = \frac{1}{2}\pi$. The case $\lambda = 1$ is exceptional, having the undesirable property that the parametric speed (2) vanishes at both end points: $\sigma(0) = \sigma(1) = 0$. The end–point curvature magnitude

$$|\kappa(0)| \;=\; |\kappa(1)| \;=\; \frac{2\,\lambda}{(1-\lambda)^2}$$

is formally infinite in this case, reflecting the fact that the graph of $\mathbf{r}(\xi)$ for unrestricted ξ is a *multiply–traced straight line*, that instantaneously reverses direction at the end points $\xi = 0$ and $\xi = 1$.

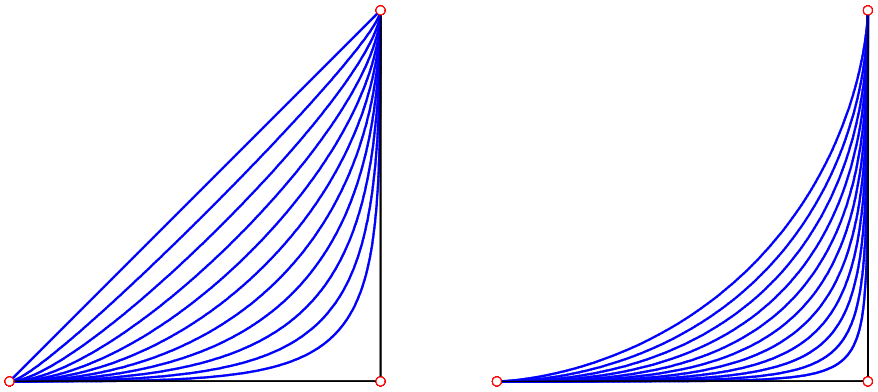

Figure 2: Corner curves of degree 3 (left) and degree 4 (right) for the turning angle $\theta = \frac{1}{2}\pi$ and the sequence of parameter values $\lambda = 0.0, 0.1, \ldots, 1.0$.

3.3 The case $n = 4$

To achieve a G^2 connection with the incoming/outgoing linear segments, we require $\kappa(0) = \kappa(1) = 0$. This can be achieved with minimum degree $n = 4$, and one can verify from the expression for $\kappa(\xi)$ in (3) that this implies that $\mathbf{p}_0, \mathbf{p}_1, \mathbf{p}_2$ must be colinear, and $\mathbf{p}_2, \mathbf{p}_3, \mathbf{p}_4$ must be colinear. For a symmetric corner curve, the control points must therefore be of the form

$$\mathbf{p}_0 \,=\, (-1,0)\,, \quad \mathbf{p}_1 \,=\, \lambda(-1,0)\,, \quad \mathbf{p}_2 \,=\, (0,0)\,,$$

$$\mathbf{p}_3 \,=\, \lambda(\cos\theta, \sin\theta)\,, \quad \mathbf{p}_4 \,=\, (\cos\theta, \sin\theta)\,,$$

where $\lambda \in [\,0,1\,]$ is a free parameter. For the quartic corner curve specified by these control points, the polynomials $f(\xi)$ and $g(\xi)$ in (7) are of degree 6 and 4, with Bernstein coefficients

$$f_0 = f_6 = 16\,(1-\lambda)^2\,, \quad f_1 = f_5 = 16\,(1-\lambda)\lambda\,,$$

$$f_2 = f_4 = \frac{16}{5}(\cos\theta\, 2(1-\lambda)\lambda + 3\,\lambda^2)\,, \quad f_3 = \frac{8}{5}\cos\theta\,((1-\lambda)^2 + 9\,\lambda^2)\,,$$

and

$$g_0 = g_4 = 0\,, \quad g_1 = g_3 = 24\,\sin\theta\,(1-\lambda)\lambda\,, \quad g_2 = 8\,\sin\theta\,((1-\lambda)^2 + 3\,\lambda^2)\,.$$

Hence, the quantities (4) have the values

$$\delta_{\mathrm{m}} \,=\, \frac{|\sin\frac{1}{2}\theta\,|}{8}\,(4\,\lambda + 1)\,, \quad \kappa_{\mathrm{m}} \,=\, \frac{6\sqrt{2}\,|\sin\theta\,|}{(1+\cos\theta)^{3/2}}\,\frac{1}{(2\,\lambda+1)^2}\,. \tag{9}$$

Note that, with $\theta \neq 0$, we have

$$\frac{\mathrm{d}\delta_{\mathrm{m}}}{\mathrm{d}\lambda} \,=\, \frac{|\sin\frac{1}{2}\theta\,|}{2} \,>\, 0 \quad \text{and} \quad \frac{\mathrm{d}\kappa_{\mathrm{m}}}{\mathrm{d}\lambda} \,=\, -\,\frac{24\sqrt{2}\,|\sin\theta\,|}{(1+\cos\theta)^{3/2}}\,\frac{1}{(2\,\lambda+1)^3} \,<\, 0\,.$$

Examples of these degree 4 corner curves are shown in Figure 2. As in the case $n = 3$, note that δ_{m} is monotone–increasing with λ, having its minimum value when $\lambda = 0$ with $\mathbf{p}_1 = \mathbf{p}_2 = \mathbf{p}_3 = (0, 0)$, whereas κ_{m} is monotone–decreasing with λ, having its minimum value when $\lambda = 1$ with $\mathbf{p}_0 = \mathbf{p}_1 = (-1, 0)$ and $\mathbf{p}_2 = \mathbf{p}_3 = (\cos\theta, \sin\theta)$. For the case $\lambda = 1$, the parametric speed (2) again vanishes at both end points, $\sigma(0) = \sigma(1) = 0$, as seen from the coefficients of the polynomial $f(\xi)$. The polynomial $g(\xi)$ also vanishes at both end points, but application of l'Hôpital's rule indicates that the curvature has the finite value 0 (as expected from the imposition of G^2 continuity).

3.4 The case $n = 5$

To achieve a G^2 connection using a quintic curve, the control points $\mathbf{p}_0, \mathbf{p}_1, \mathbf{p}_2$ must be colinear, and $\mathbf{p}_3, \mathbf{p}_4, \mathbf{p}_5$ must be colinear — i.e., we must have

$$\mathbf{p}_0 \,=\, (-1, 0)\,, \quad \mathbf{p}_1 \,=\, \lambda(-1, 0)\,, \quad \mathbf{p}_2 \,=\, \mu(-1, 0)\,,$$

$$\mathbf{p}_3 \,=\, \mu(\cos\theta, \sin\theta)\,, \quad \mathbf{p}_4 \,=\, \lambda(\cos\theta, \sin\theta)\,, \quad \mathbf{p}_5 \,=\, (\cos\theta, \sin\theta)\,,$$

$\lambda, \mu \in [\,0, 1\,]$ being free parameters with $\lambda \geq \mu$. In this case, the polynomials $f(\xi)$ and $g(\xi)$ in (7) are of degree 8 and 6 in ξ, respectively. For brevity, we omit their coefficients, but observe that we again have $\mathbf{r}'(0) = \mathbf{r}'(1) = \mathbf{0}$ when $\lambda = 1$. The quantities (4) can be expressed as

$$\delta_{\mathrm{m}} \,=\, \frac{|\sin\frac{1}{2}\theta\,|}{16}\,(5\,\lambda + 10\,\mu + 1)\,, \quad \kappa_{\mathrm{m}} \,=\, \frac{64\sqrt{2}\,|\sin\theta\,|}{5\,(1+\cos\theta)^{3/2}}\,\frac{\lambda - 2\,\mu + 1}{(3\,\lambda + 2\,\mu + 1)^2}\,.$$

Note that δ_{m} is monotone–increasing with λ and μ, and thus has its minimum value when $\lambda = \mu = 0$, i.e., $\mathbf{p}_1 = \mathbf{p}_2 = \mathbf{p}_3 = \mathbf{p}_4 = (0, 0)$. The behavior of κ_{m} is more complicated, as is evident from its partial derivatives $\partial\kappa_{\mathrm{m}}/\partial\lambda$ and $\partial\kappa_{\mathrm{m}}/\partial\mu$, which are proportional to

$$\frac{14\,\mu - 3\,\lambda - 5}{(3\,\lambda + 2\,\mu + 1)^3} \qquad \text{and} \qquad \frac{4\,\mu - 10\,\lambda - 6}{(3\,\lambda + 2\,\mu + 1)^3}\,.$$

The condition $\partial\kappa_{\mathrm{m}}/\partial\lambda = \partial\kappa_{\mathrm{m}}/\partial\mu = 0$ identifies a local stationary point of κ_{m} at $(\lambda, \mu) = (-1/2, 1/4)$ but this lies outside the domain $0 \leq \mu \leq \lambda \leq 1$.

3.5 The case $n = 6$

To achieve a G^3 connection with the incoming/outgoing linear segments, we must have $\kappa(0) = \mathrm{d}\kappa/\mathrm{d}s(1) = 0$ and $\kappa(1) = \mathrm{d}\kappa/\mathrm{d}s(0) = 0$. This requires a curve of minimum degree 6. One can verify from expressions (3) that these

conditions imply that $\mathbf{p}_0, \mathbf{p}_1, \mathbf{p}_2, \mathbf{p}_3$ must be colinear, and $\mathbf{p}_3, \mathbf{p}_4, \mathbf{p}_5, \mathbf{p}_6$ must be colinear — i.e., we must have

$$\mathbf{p}_0 \,=\, (-1,0)\,, \quad \mathbf{p}_1 \,=\, \lambda(-1,0)\,, \quad \mathbf{p}_2 \,=\, \mu(-1,0)\,, \quad \mathbf{p}_3 \,=\, (0,0)\,,$$

$$\mathbf{p}_4 \,=\, \mu(\cos\theta, \sin\theta)\,, \quad \mathbf{p}_5 \,=\, \lambda(\cos\theta, \sin\theta)\,, \quad \mathbf{p}_6 \,=\, (\cos\theta, \sin\theta)\,,$$

$\lambda, \mu \in [\,0,1\,]$ being free parameters with $\lambda \geq \mu$. In this case, the polynomials $f(\xi)$ and $g(\xi)$ in (7) are of degree 10 and 8 in ξ, respectively. For brevity, we omit their coefficients, but note again that $\mathbf{r}'(0) = \mathbf{r}'(1) = \mathbf{0}$ when $\lambda = 1$. The quantities (4) can be expressed as

$$\delta_{\mathrm{m}} \,=\, \frac{|\sin\frac{1}{2}\theta\,|}{32}\,(6\,\lambda + 15\,\mu + 1)\,, \quad \kappa_{\mathrm{m}} \,=\, \frac{80\sqrt{2}\,|\sin\theta\,|}{3\,(1+\cos\theta)^{3/2}}\,\frac{2\,\lambda - \mu + 1}{(4\,\lambda + 5\,\mu + 1)^2}\,.$$

Again, δ_{m} is monotone–increasing with λ and μ, and has its minimum value when $\lambda = \mu = 0$, i.e., $\mathbf{p}_1 = \mathbf{p}_2 = \mathbf{p}_3 = \mathbf{p}_4 = \mathbf{p}_5 = (0,0)$. The behavior of κ_{m} is more complicated: its partial derivatives with respect to λ and μ are proportional to

$$\frac{18\,\mu - 8\,\lambda - 6}{(4\,\lambda + 5\,\mu + 1)^3} \qquad \text{and} \qquad \frac{5\,\mu - 24\,\lambda - 11}{(4\,\lambda + 5\,\mu + 1)^3}\,.$$

The condition $\partial\kappa_{\mathrm{m}}/\partial\lambda = \partial\kappa_{\mathrm{m}}/\partial\mu = 0$ identifies a local stationary point of κ_{m} at $(\lambda, \mu) = (-3/7, 1/7)$ but this lies outside the domain $0 \leq \mu \leq \lambda \leq 1$.

4 Corner curve optimization

Ideally, a corner blending curve should exhibit a small deviation δ_{m} from the original sharp corner point, and a small mid–point curvature magnitude κ_{m}. However, minimizing these quantities incurs conflicting demands on the free parameters defining the corner curve, so a compromise must be sought.

In optimizing a corner blending curve specified by the canonical data (1), a dimensionless objective function must be adopted, to ensure that the curve scales uniformly to any desired length $L = \|\mathbf{p}_c - \mathbf{p}_i\| = \|\mathbf{p}_o - \mathbf{p}_c\|$ of the corner edges. The simplest choice is the product $\kappa_{\mathrm{m}}\delta_{\mathrm{m}}$, but since κ_{m} has a stronger dependence on the free parameters than δ_{m}, it dominates in determining their optimal values. In the cases $n = 3$ and $n = 4$, for example, it can be verified from (8) and (9) that

$$\frac{\mathrm{d}}{\mathrm{d}\lambda}\,\kappa_{\mathrm{m}}\delta_{\mathrm{m}} \,<\, 0 \quad \text{for } \lambda \in [\,0,1\,]$$

so $\kappa_{\mathrm{m}}\delta_{\mathrm{m}}$ is minimized when $\lambda = 1$. With this value, however, the corner curve has a singular parameterization at its end points, since we have $\mathbf{p}_0 = \mathbf{p}_1$ and

$\mathbf{p}_{n-1} = \mathbf{p}_n$ and thus $\sigma(0) = \sigma(1) = 0$. Furthermore, the minimization of an objective function in which $\kappa_{\rm m}$ dominates is observed to frequently produce an undesirable bimodal curvature profile, exhibiting higher curvatures near the end points than at the mid point.

To preclude the possibility of singular solutions with $\sigma(0) = \sigma(1) = 0$, we introduce a dimensionless term dependent on the variation of the parametric speed in the objective function. The arc length S of the corner curve $\mathbf{r}(\xi)$ is defined in terms of the parametric speed (2) by

$$S \;=\; \int_0^1 \sigma(\xi)\,\mathrm{d}\xi\,,$$

and the mean value of $\sigma(\xi)$ is $\bar{\sigma} = S$. A dimensionless measure of the mean square deviation of $\sigma(\xi)$ about $\bar{\sigma}$ is then defined through the expression

$$\gamma \;=\; \frac{1}{S^2}\int_0^1 [\,\sigma(\xi) - \bar{\sigma}\,]^2\,\mathrm{d}\xi \;=\; \frac{1}{S^2}\int_0^1 \sigma^2(\xi)\,\mathrm{d}\xi - 1\,. \tag{10}$$

Note that S can be exactly computed for PH curves, but general polynomial curves require a numerical quadrature. However, the integral on the right in (10) admits an exact evaluation for any polynomial curve. Although (10) is not an intrinsic shape measure, including it in the objective function produces corner curves closer to the ideal of an arc–length parameterization.

Instead of using the product $\kappa_{\rm m}\delta_{\rm m}$, we introduce individual dimensionless measures of $\kappa_{\rm m}$ and $\delta_{\rm m}$ by dividing them by the values

$$\bar{\kappa}_{\rm m} \;=\; \frac{|\,\theta\,|}{S} \qquad \text{and} \qquad \bar{\delta}_{\rm m} \;=\; \tfrac{1}{2}\,|\sin\tfrac{1}{2}\theta\,|\,.$$

These are the averages of $\kappa_{\rm m}$ and $\delta_{\rm m}$ for the two "extreme" solutions identified in Section 2, namely, the piecewise–linear path from $\mathbf{p}_i$ to $\mathbf{p}_o$ through $\mathbf{p}_c$, and the direct short–cut linear path from $\mathbf{p}_i$ to $\mathbf{p}_o$. We then define the objective function

$$f \;=\; a\,(\delta_{\rm m}/\bar{\delta}_{\rm m}) \;+\; b\,(\kappa_{\rm m}/\bar{\kappa}_{\rm m}) \;+\; (1-a-b)\,\gamma\,, \tag{11}$$

where a, b are non–negative weights such that $a + b \le 1$. For given choices of a, b this is to be minimized with respect to the free parameters characterizing the corner curve $\mathbf{r}(\xi)$.

5 Optimization algorithm

For polynomial curves of degree 3 and 4, the optimal corner curve is found by minimizing a univariate function on the domain $\lambda \in [\,0, 1\,]$. For curves of degree 5 and 6, however, the optimal solution is identified by minimizing a

convex objective function in two variables, λ and μ, subject to linear (equality and inequality) constraints. In both instances, the optimization procedure has been implemented in Matlab by using the solver routines in the Matlab Optimization toolbox. We give below just a brief synopsis of the main ideas — see [10, 12, 22] for complete details.

5.1 Univariate objective function

In this case, the algorithm employs a combination of the Successive Parabolic Interpolation method and the Golden Section Search. Successive Parabolic Interpolation has a superlinear convergence rate, and is based on successive fitting of parabolas to a unimodal function at three unique points. At each iteration, the "oldest" point is replaced by the extremum of the current parabola fit. Only function values (no derivatives) are used, and when the method converges, its convergence rate is ~ 1.325. However, it may happen that the minimum does not lie in the interval determined by the three points, and in this case two steps of Golden Section Search are usually employed. This identifies the minimum of a strictly unimodal function by successively narrowing an interval in which the minimum is known to exist. It derives its name from the fact that it uses function values at sets of three points whose distances form the golden ratio, $(\sqrt{5}-1)/2 \approx 0.6180$. It is guaranteed to identify the minimum, and again does not require function derivatives. As the interval width is only reduced by the factor of 0.618 at each step, the method is just linearly convergent.

The above algorithm has been implemented in the Matlab routine "`fminbnd`," a local minimizer of a univariate objective function over a given interval.

5.2 Multivariate objective function

Among available algorithms for solving constrained optimization problems of the form

$$\begin{cases} \min_{\mathbf{x}} f(\mathbf{x}) \\ h_i(\mathbf{x}) = 0, \quad i = 1, \ldots, n_e, \\ g_i(\mathbf{x}) \leq 0, \quad i = 1, \ldots, n_i, \end{cases} \tag{12}$$

in a set of variables $\mathbf{x}$, we opt for the Sequential Quadratic Programming (SQP) method. SQP is considered a state–of–the–art nonlinear programming method — see, for instance, [12]. It belongs to the class of methods that solve the Karush–Kuhn–Tucker (KKT) equations. The main idea behind the KKT equations — as with the Lagrange multiplier method — is to combine the objective function and constraints in a single minimization problem, with the equality constraints multiplied by factors ρ_i, $i = 1, \ldots, n_e$ and the inequality

constraints by factors τ_i, $i = 1, \ldots, n_i$ (the so called KKT multipliers, often also called Lagrange multipliers). The problem then becomes

$$\begin{cases} \nabla f(\mathbf{x}) + \displaystyle\sum_{i=1}^{n_e} \nabla \rho_i \, h_i(\mathbf{x}) + \sum_{i=1}^{n_i} \nabla \tau_i \, g_i(\mathbf{x}) = 0 \\ \tau_i \, g_i(\mathbf{x}) = 0 \,, \quad i = 1, \ldots, n_i \,, \\ \tau_i \geq 0 \,, \quad i = 1, \ldots, n_i \,, \end{cases} \tag{13}$$

in addition to the original constraints in (12). Satisfaction of these equations is a necessary condition for solution of a constrained optimization problem. If the problem is strictly convex, i.e., $f(\mathbf{x})$ is strictly convex and $h_i(\mathbf{x})$, $g_i(\mathbf{x})$ define a convex region, the KKT equations are both necessary and sufficient for a global optimal solution.

SQP methods to solve the non–linear system (13) mimic Newton's method. We briefly summarize here the main steps (see [22] for complete details). The basic structure of an SQP method involves *major* and *minor* iterations. Its name comes from the fact that a quadratic programming (QP) subproblem is solved at each major iteration, to find a direction for a line search procedure. Writing $\mathbf{h} = (h_1, \ldots, h_{n_e})^T$ and $\mathbf{g} = (g_1, \ldots, g_{n_i})^T$, the subproblem objective function is a quadratic approximation of the Lagrangian function

$$\mathcal{L}(\mathbf{x}, \boldsymbol{\rho}, \boldsymbol{\tau}) \;=\; f(\mathbf{x}) - \boldsymbol{\rho}^T \mathbf{h}(\mathbf{x}) - \boldsymbol{\tau}^T \mathbf{g}(\mathbf{x}) \,, \tag{14}$$

and the constraints are linearizations of the constraints in (12). Note that the bound constraints are expressed as inequalities.

In the present context, the method is greatly simplified since the problem is convex, and the constraints are all linear. Consequently, fast convergence is observed in practice, with the stopping criterion being met in a few iterations.

Since we employ the Matlab Optimization toolbox, the routine that best meets our requirements is "`fmincon`," which deals with nonlinear constrained optimization. In addition, we use the option "`sqp`" to enforce the routine to employ the SQP methods described above. This, together with the fact that we are dealing with problems of modest size, ensures a fast convergence rate. Concerning the starting values for the optimization parameters, we note that the problem is not very sensitive to their choice, so we simply set them equal to zero (recall that they must both be in the interval $[\,0, 1\,]$).

6 Computed examples

Since different applications typically entail different criteria concerning what constitutes an "optimal" corner shape, the approach adopted herein does not purport to identify a universal shape optimality criterion. Certain properties,

a	b	λ	δ_{m}	κ_{m}	γ
0.0	0.0	0.4751	0.4287	0.9091	1.0174×10^{-5}
0.1	0.0	0.3295	0.3515	1.4304	1.2696×10^{-2}
0.4	0.0	0.0001	0.1768	3.7705	1.0845×10^{-1}
0.0	0.1	0.6336	0.5128	0.5178	1.7649×10^{-2}
0.8	0.2	0.2611	0.3153	1.7520	2.6286×10^{-2}

Table 1: Numerical results for cubic corner curves with turning angle $\theta = \frac{1}{2}\pi$.

such as a unimodal curvature, are likely desirable in all cases, but minimum curvature may be favored over minimum deviation in some applications, and vice–versa for other applications. The optimization objective function offers the flexibility (by adjusting the weights) to tailor the measure of corner curve shape quality to suit the needs of particular applications.

For brevity, we focus here on the representative turning angles $\theta = \frac{1}{4}\pi$, $\frac{1}{2}\pi$, $\frac{3}{4}\pi$. Results for degrees $n = 3, 4, 5, 6$ are presented with turning angle $\theta = \frac{1}{2}\pi$, and for degrees $n = 4, 5$ with the angles $\theta = \frac{1}{4}\pi$ and $\frac{3}{4}\pi$. In practice, the cases $n = 4$ and 5, which provide G^2 continuity with one and two free parameters, may be considered preferable — the degree 3 corner curve provides only G^1 continuity, while on the other hand the G^3 continuity of the degree 6 corner curve can incur severe curvature variation between the end points.

6.1 Turning angle $\theta = \frac{1}{2}\pi$

We begin with the right–angle corner, $\theta = \frac{1}{2}\pi$. Figure 3 shows representative examples of optimized G^1 cubic corner curves for this turning angle, obtained with various weights a, b in the objective function (11). Table 1 indicates the chosen weights, together with the optimum values for the sole parameter λ, and the resulting values of δ_{m}, κ_{m}, γ. With $a = b = 0$, the objective function contains only the term (10). This results in a very low value of γ, reflecting a near–uniform parameterization, and the curvature is nearly constant (though slightly lower at the center than at the end points). Fixing $b = 0$ and increasing a to 0.1 and 0.4 yields "sharper" corner curves, with smaller δ_{m} but substantially larger κ_{m}, and in the case $a = 0.4$ the solution is nearly singular, with λ approaching 0. The case $a = 0$, $b = 0.1$ illustrates the strong influence of the κ_{m} term in (11) — the resulting corner curve is very "flat" in the center, with very high curvature at the end points. Finally, the case $a = 0.8$, $b = 0.2$ shows a result obtained without the term (10) in the objective function (11) — the corner curve has a smooth unimodal curvature profile, with reasonable values for δ_{m} and κ_{m}.

Results for optimized G^2 quartic corner curves are presented in Figure 4 and Table 2. The choice $a = b = 0$ is again seen to yield an excellent result,

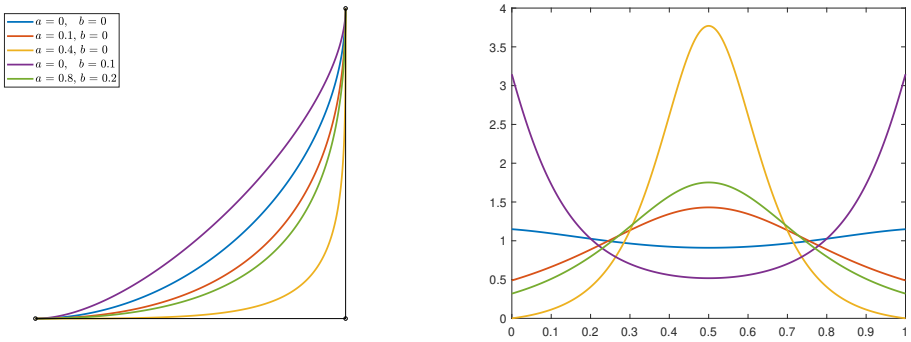

Figure 3: Optimized cubic corner curves with turning angle $\frac{1}{2}\pi$ and different values of the weights a, b (left), and the corresponding curvature plots (right).

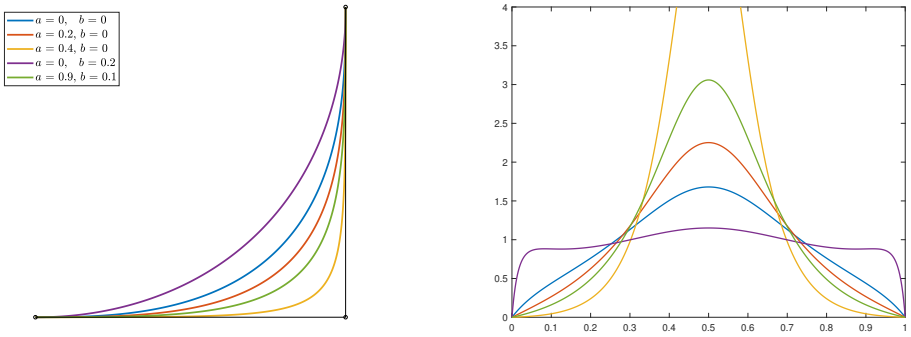

Figure 4: Optimized quartic corner curves with turning angle $\frac{1}{2}\pi$ and different values of the weights a, b (left), and the corresponding curvature plots (right).

a	b	λ	δ_{m}	κ_{m}	γ
0.0	0.0	0.6237	0.3089	1.6799	1.3847×10^{-3}
0.2	0.0	0.4706	0.2548	2.2517	2.1178×10^{-2}
0.4	0.0	0.0925	0.1211	6.0429	2.0295×10^{-1}
0.0	0.2	0.8576	0.3916	1.1510	5.5882×10^{-2}
0.9	0.1	0.3327	0.2060	3.0593	6.8728×10^{-2}

Table 2: Numerical values for quartic corner curves and turning angle $\theta = \frac{1}{2}\pi$.

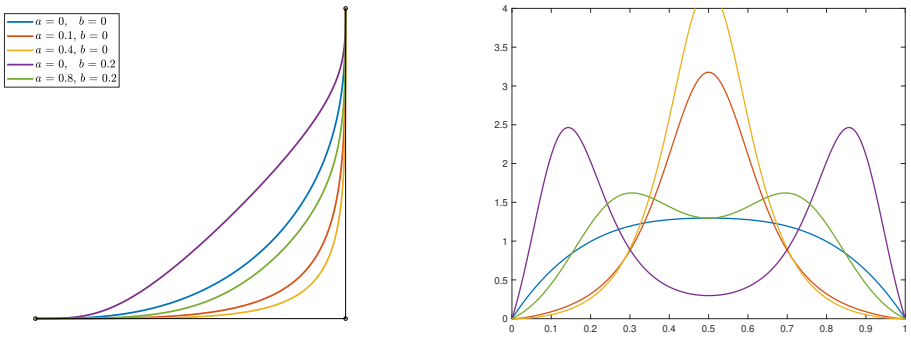

Figure 5: Optimized quintic corner curves with turning angle $\frac{1}{2}\pi$ and different values of the weights a, b (left), and the corresponding curvature plots (right).

with reasonable values for δ_{m} and κ_{m}, near–uniform parameterization, and a unimodal curvature profile. On fixing $b = 0$ and increasing a to 0.2 and 0.4, the curvature remains unimodal with a smaller δ_{m} and larger κ_{m}. However, the case $a = 0$ and $b = 0.2$ produces a rather strange curvature profile that is actually trimodal. Finally, the weights $a = 0.9$ and $b = 0.1$ yield a relatively low δ_{m} value and correspondingly higher κ_{m} value.

a	b	λ	μ	δ_{m}	κ_{m}	γ
0.0	0.0	0.6730	0.3441	0.3450	1.2971	3.2195×10^{-7}
0.1	0.0	0.7059	0.0000	0.2002	3.1768	1.7527×10^{-2}
0.4	0.0	0.5106	0.0000	0.1570	4.2658	6.5916×10^{-2}
0.0	0.2	0.6812	0.6812	0.4958	0.2973	2.8929×10^{-2}
0.8	0.2	0.3858	0.3858	0.3000	1.2958	8.4877×10^{-2}

Table 3: Numerical values for quintic corner curves and turning angle $\theta = \frac{1}{2}\pi$.

With the G^2 quintic corners, two free parameters are available to optimize the objective function (11). The results are presented in Figure 5 and Table 3. Comparing with Figure 4, the curvature profile for the $a = b = 0$ corner curve appears superior (being strictly convex) than for the corresponding quartic curve. Increasing a to 0.1 and 0.4 with $b = 0$ yields smaller δ_{m} and larger κ_{m} values, preserving a unimodal curvature profile — the optimum μ values in these cases are zero to machine precision, so that $\mathbf{p}_2 = \mathbf{p}_3 = (0, 0)$. With $a = 0.0$ and $b = 0.2$ the corner curve has a very "flat" interior, with strong curvature near the end points (although we still have $\kappa(0) = \kappa(1) = 0$). The case $a = 0.8$ and $b = 0.2$ yields a less pronounced bimodal curvature.

Finally, Figure 6 and Table 4 present results for the G^3 sextic corners (with two free parameters). The cases $a = b = 0$ and $a = 0.8$, $b = 0.2$ yield

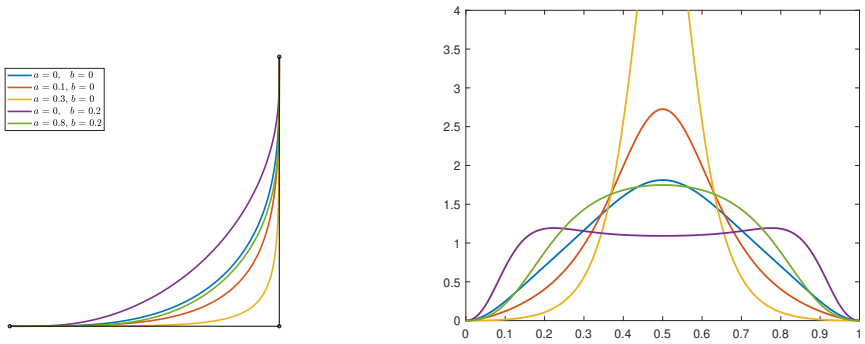

Figure 6: Optimized sextic corner curves with turning angle $\frac{1}{2}\pi$ and different values of the weights a, b (left), and the corresponding curvature plots (right).

a	b	λ	μ	δ_{m}	κ_{m}	γ
0.0	0.0	0.7054	0.4978	0.2806	1.8115	1.4993×10^{-4}
0.1	0.0	0.7340	0.3065	0.2210	2.7258	9.8866×10^{-3}
0.3	0.0	0.7429	0.0000	0.1206	5.9430	6.2701×10^{-2}
0.0	0.2	0.7535	0.7535	0.3717	1.0922	3.7542×10^{-2}
0.8	0.2	0.5265	0.5265	0.2664	1.7480	3.6332×10^{-2}

Table 4: Numerical values for sextic corner curves and turning angle $\theta = \frac{1}{2}\pi$.

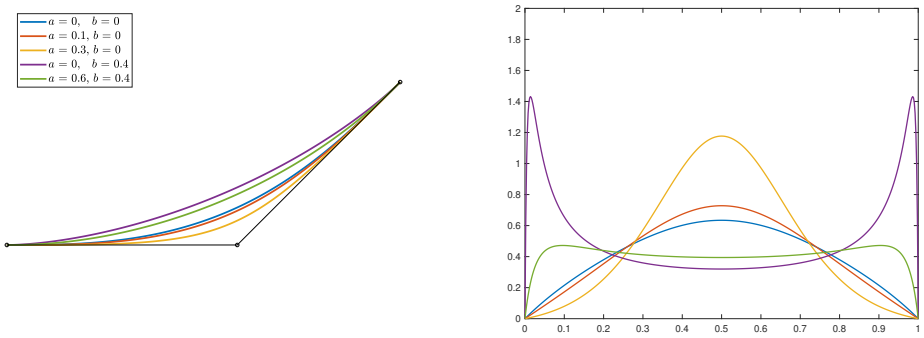

Figure 7: Optimized quartic corner curves with turning angle $\frac{1}{4}\pi$ and different values of the weights a, b (left), and the corresponding curvature plots (right).

a	b	λ	δ_{m}	κ_{m}	γ
0.0	0.0	0.5298	0.1492	0.6342	5.3642×10^{-5}
0.1	0.0	0.4611	0.1361	0.7280	3.8809×10^{-3}
0.3	0.0	0.2560	0.0968	1.1768	5.9633×10^{-2}
0.0	0.4	0.9498	0.2296	0.3200	1.5012×10^{-1}
0.6	0.4	0.8060	0.2021	0.3943	6.4128×10^{-2}

Table 5: Numerical values for quartic corner curves and turning angle $\theta = \frac{1}{4}\pi$.

similar favorable curves, while increasing a with $b = 0$ gives a smaller δ_{m} and larger κ_{m}. With $a = 0, b = 0.2$ a bimodal curvature profile results.

6.2 Turning angles $\theta = \frac{1}{4}\pi$ and $\frac{3}{4}\pi$

For the turning angles $\theta = \frac{1}{4}\pi$ and $\frac{3}{4}\pi$, we restrict our attention to the degree 4 and 5 corner curves, which are the best suited to practical use. Results for the optimized quartic and quintic corner curves with $\theta = \frac{1}{4}\pi$ are presented in Figure 7 and Table 5 and in Figure 8 and Table 6, respectively.

For quartic curves with $\theta = \frac{1}{4}\pi$, the choice $a = b = 0$ yields an excellent result, with a smooth unimodal curvature and reasonable values of δ_{m} and κ_{m}. Increasing a to 0.1 decreases δ_{m} and increases κ_{m} somewhat, and increasing to $a = 0.3$ yields larger changes in these quantities. For $a = 0.6$ and $b = 0.4$, a bimodal curvature profile begins to develop, and becomes very pronounced when $a = 0.0$ and $b = 0.4$, so the term γ has zero weight in (11). Quintic corner curves with $\theta = \frac{1}{4}\pi$ are qualitatively similar, with unimodal curvature if $b = 0$ and bimodal curvature if $b \neq 0$. The very small γ values obtained when $a = b = 0$, for both the quartic and quintic corner curves, indicate that they closely approximate a (scaled) arc–length parameterization.

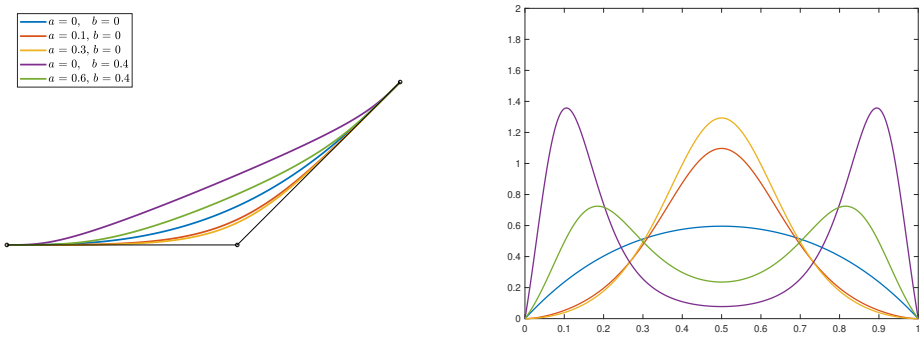

Figure 8: Optimized quintic corner curves with turning angle $\frac{1}{4}\pi$ and different values of the weights a, b (left), and the corresponding curvature plots (right).

a	b	λ	μ	δ_{m}	κ_{m}	γ
0.0	0.0	0.6162	0.2359	0.1540	0.5957	4.4229×10^{-8}
0.1	0.0	0.6443	0.0000	0.1010	1.0971	6.3183×10^{-3}
0.4	0.0	0.4553	0.0000	0.0784	1.4920	5.2457×10^{-2}
0.0	0.4	0.7158	0.7158	0.2807	0.0778	7.7909×10^{-2}
0.6	0.4	0.4986	0.4986	0.2028	0.2358	8.2103×10^{-3}

Table 6: Numerical values for quintic corner curves and turning angle $\theta = \frac{1}{4}\pi$.

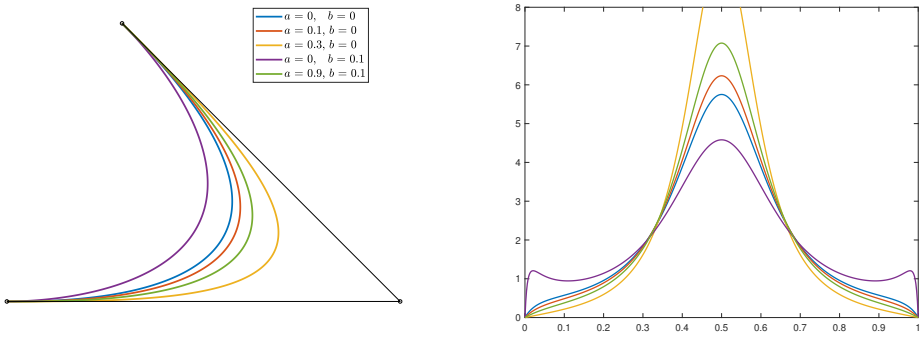

Figure 9: Optimized quartic corner curves with turning angle $\frac{3}{4}\pi$ and different values of the weights a, b (left), and the corresponding curvature plots (right).

a	b	λ	δ_{m}	κ_{m}	γ
0.0	0.0	0.7827	0.4770	5.7515	1.8447×10^{-2}
0.1	0.0	0.7321	0.4537	6.2336	2.1340×10^{-2}
0.3	0.0	0.4944	0.3439	9.5696	9.1073×10^{-2}
0.0	0.1	0.9371	0.5484	4.5820	5.2798×10^{-2}
0.9	0.1	0.6564	0.4187	7.0761	3.5010×10^{-2}

Table 7: Numerical values for quartic corner curves and turning angle $\theta = \frac{3}{4}\pi$.

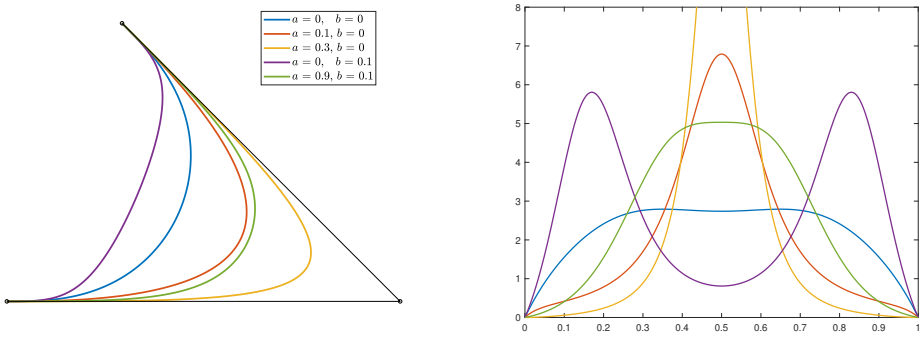

Figure 10: Optimized quintic corner curves with turning angle $\frac{3}{4}\pi$ and various values of the weights a, b (left), and the corresponding curvature plots (right).

Results for the severe turning angle $\theta = \frac{3}{4}\pi$ are presented in Figure 9 and Table 7 for quartics, and in Figure 10 and Table 8 for quintics. The quartics with $a = 0, 0.1, 0.3$ and $b = 0$ show unimodal curvatures with decreasing δ_{m} and increasing κ_{m}. The case $a = 0.9$, $b = 0.1$ is similar to $a = 0.1$, $b = 0.0$ but $a = 0$, $b = 0.1$ produces a trimodal curvature. The $\theta = \frac{3}{4}\pi$ quintics are unusual, in that the choice $a = b = 0$ deviates (slightly) from the unimodal curvature at smaller angles. For $a = 0.1, 0.3$ with $b = 0$, the curvature is again unimodal, with large κ_{m} values. For $a = 0$, $b = 0.1$ the curve has a "flat" interior and strong curvature near the end points. Finally, for $a = 0.9$, $b = 0.1$ the curvature is unimodal, with a near–constant central curvature.

a	b	λ	μ	δ_{m}	κ_{m}	γ
0.0	0.0	0.7899	0.5547	0.6061	2.7389	2.0610×10^{-5}
0.1	0.0	0.7867	0.2602	0.4351	6.7907	2.5705×10^{-2}
0.3	0.0	0.6701	0.0000	0.2512	14.883	8.3100×10^{-2}
0.0	0.1	0.7658	0.7658	0.7211	0.8109	2.0968×10^{-2}
0.9	0.1	0.4135	0.4135	0.4159	5.0327	2.2237×10^{-1}

Table 8: Numerical values for quintic corner curves and turning angle $\theta = \frac{3}{4}\pi$.

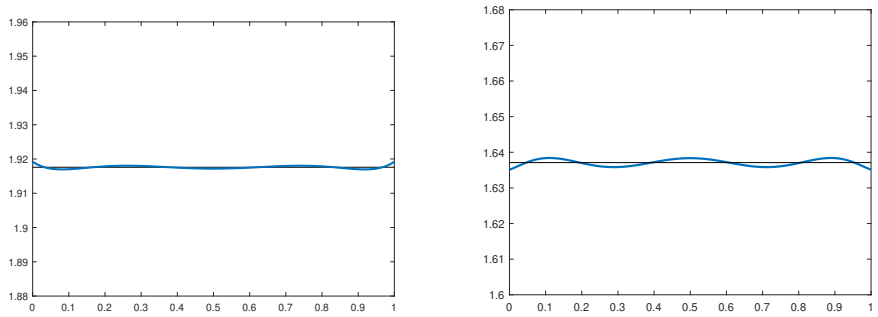

Figure 11: Variation of the parametric speed (2) about the mean value $\bar{\sigma} = S$ for the optimized quintic corner curves with turning angles $\frac{1}{4}\pi$ (left) and $\frac{1}{2}\pi$ (right) with weights $a = b = 0$, i.e., only the term (10) in (11) is minimized.

δ^*	λ	μ	κ_m	γ
0.20	0.5668	0.4528	0.2918	4.4819×10^{-3}
0.17	0.5992	0.3112	0.4793	5.3864×10^{-3}
0.15	0.6204	0.2170	0.6271	3.3948×10^{-5}
0.10	0.6362	0.0000	1.1099	6.9388×10^{-3}
0.05	0.2181	0.0000	2.5543	2.0113×10^{-1}

Table 9: Quintic corner curves with $\theta = \frac{1}{4}\pi$ and prescribed δ_{m} values.

Figure 11 illustrates the variation of the parametric speed (2) about the mean value $\bar{\sigma} = S$ for optimized quintic corner curves with $a = b = 0$ and the turning angles $\theta = \frac{1}{4}\pi$ and $\frac{1}{2}\pi$. It is seen that emphasizing the term (10) in the objective function (11) results in not only reasonable values for δ_{m} and κ_{m}, but also close approximation of the (scaled) arc–length parameterization.

6.3 Constrained corner curves

As a variant of the optimization procedure, we consider minimization of (10) with the imposition of a specified value for the deviation δ_{m} as a constraint. This problem is important in applications where the rounded corners should not deviate by more than a given tolerance from a prescribed piecewise–linear locus. We focus on the quintic corner curves, since the introduction of this constraint leaves no free optimization parameters when $n < 5$. Note that, since the expression for δ_{m} is linear in λ and μ, we may eliminate one of these parameters to obtain a univariate optimization problem.

Figure 12 and Table 9 presents results for optimized quintic corner curves with turning angle $\theta = \frac{1}{4}\pi$ and several values of the normalized displacement $\delta^* := \delta/\bar{\delta}$. The ability to specify a uniform sequence of δ^* values yields a more

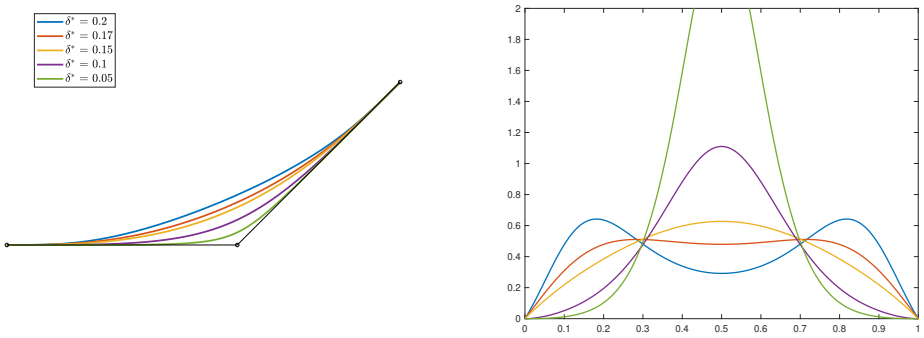

Figure 12: Optimized quintic corner curves for $\theta = \frac{1}{4}\pi$ and different values of the normalized deviation δ^* (left), with corresponding curvature plots (right).

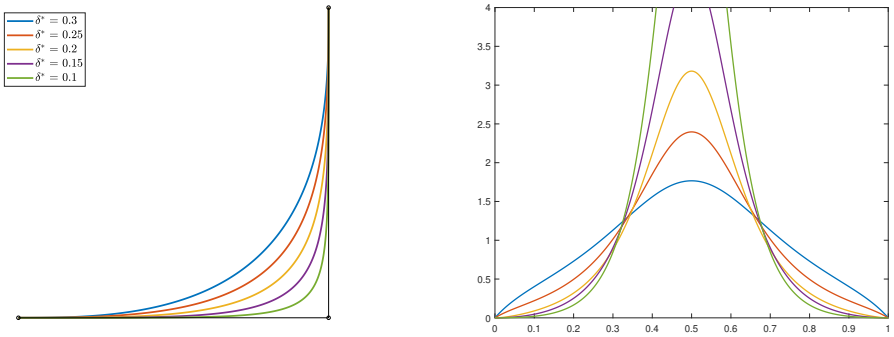

Figure 13: Optimized quintic corner curves for $\theta = \frac{1}{2}\pi$ and different values of the normalized deviation δ^* (left), with corresponding curvature plots (right).

predictable sequence of corner curve shapes, and κ_{m} values, than modifying the weights a, b in (11). Figure 13 and Table 10 present analogous results for $\theta = \frac{1}{2}\pi$, and Figure 14 and Table 11 for $\theta = \frac{3}{4}\pi$. Except for the larger δ^* values, the curvature is unimodal, with larger κ_{m} values as δ^* increases.

7 Pythagorean-hodograph corner curves

Pythagorean–hodograph (PH) curves are a special class of polynomial curves [5], characterized by a *polynomial* parametric speed $\sigma(\xi)$. Consequently, the PH curves possess several advantageous properties, including exact arc length computation; versatile algorithms for real–time motion control; and favorable shape properties [5]. PH corner curves have previously been discussed in the context of G^2 blends of right–angle corners [6]; G^2 corner blends and feedrate functions for general turning angles [8, 21]; and by various other authors in

δ^*	λ	μ	κ_m	γ
0.30	0.6883	0.2347	1.7665	1.8686×10^{-3}
0.25	0.7037	0.1138	2.3969	7.9237×10^{-3}
0.20	0.7051	0.0000	3.1804	1.7586×10^{-2}
0.15	0.4788	0.0000	4.5094	7.9984×10^{-2}
0.10	0.2526	0.0000	7.3393	2.2409×10^{-1}

Table 10: Quintic corner curves with $\theta = \frac{1}{2}\pi$ and prescribed δ_{m} values.

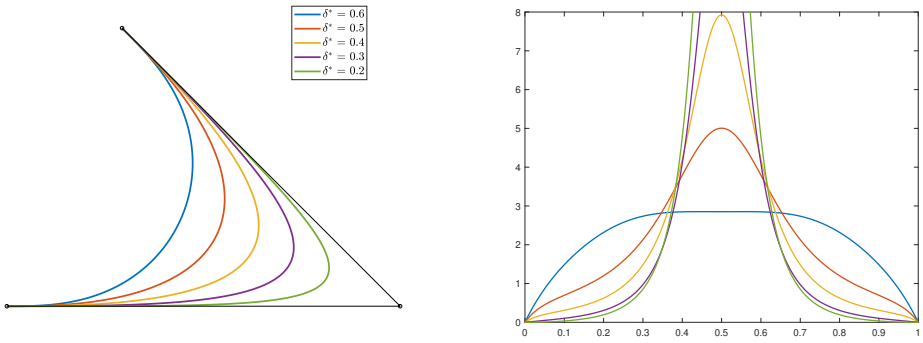

Figure 14: Optimized quintic corner curves for $\theta = \frac{3}{4}\pi$ and different values of the normalized deviation δ^* (left), with corresponding curvature plots (right).

δ^*	λ	μ	κ_m	γ
0.60	0.7901	0.5440	2.8520	6.8098×10^{-5}
0.50	0.7897	0.3711	5.0046	1.1517×10^{-2}
0.40	0.7844	0.2005	7.9255	3.4403×10^{-2}
0.30	0.7761	0.0315	12.028	6.0239×10^{-2}
0.20	0.4927	0.0000	19.627	1.5448×10^{-1}

Table 11: Quintic corner curves with $\theta = \frac{3}{4}\pi$ and prescribed $\delta_{\rm m}$ values.

the context of CNC machining applications [18, 19, 26, 27, 28, 36].

For comparison with the polynomial corner curves discussed in Section 3, we give a brief synopsis of PH corner curves of degree $3, 5, 7$ and continuity G^1, G^2, G^3 for general turning angles. For a given turning angle, these curves are essentially unique — the curve degree determines the order of continuity. In the complex representation [3], a planar PH curve of degree $n = 2m + 1$ is generated by integrating the square of a complex polynomial,

$$\mathbf{r}'(\xi) \;=\; \mathbf{w}^2(\xi)\,, \quad \mathbf{w}(\xi) \;=\; \sum_{k=0}^{m} \mathbf{w}_k \binom{m}{k} (1-\xi)^{m-k} \xi^k\,, \tag{15}$$

with coefficients $\mathbf{w}_k = u_k + \mathrm{i}\, v_k$ for $k = 0, \ldots, m$.

7.1 G^1 PH cubic corner curve

It is well–known that all planar PH cubics are segments of a unique curve — the *Tschirnhaus cubic* [5]. For the instance $m = 1$ of (15), one can verify that the G^1 boundary conditions $\mathbf{r}(0) = -1$, $\arg(\mathbf{r}'(0)) = 0$ and $\mathbf{r}(1) = \exp(\mathrm{i}\,\theta)$, $\arg(\mathbf{r}'(1)) = \theta$ for a PH cubic corner curve are satisfied with

$$\mathbf{w}_0 \;=\; \sqrt{\frac{6\cos\frac{1}{2}\theta}{2\cos\frac{1}{2}\theta + 1}}\,, \quad \mathbf{w}_1 \;=\; \sqrt{\frac{6\cos\frac{1}{2}\theta}{2\cos\frac{1}{2}\theta + 1}}\,\exp(\mathrm{i}\tfrac{1}{2}\theta)\,,$$

and with $\mathbf{p}_0 = (-1, 0)$, $\mathbf{p}_3 = (\cos\theta, \sin\theta)$ the intermediate control points are

$$\mathbf{p}_1 \;=\; \frac{(-1, 0)}{2\cos\frac{1}{2}\theta + 1}\,, \quad \mathbf{p}_2 \;=\; \frac{(\cos\theta, \sin\theta)}{2\cos\frac{1}{2}\theta + 1}\,.$$

In this case, the quantities (4) are given by

$$\delta_{\rm m} \;=\; \frac{(\cos\frac{1}{2}\theta + 2)\,|\sin\frac{1}{2}\theta\,|}{2(2\cos\frac{1}{2}\theta + 1)}\,, \quad \kappa_{\rm m} \;=\; \frac{4\,(2\cos\frac{1}{2}\theta + 1)|\tan\frac{1}{2}\theta\,|}{3\,(\cos\frac{1}{2}\theta + 1)^2}\,.$$

7.2 G^2 PH quintic corner curve

It was shown in [8] that a G^2 PH quintic corner curve defined by the instance $m = 2$ of (15), satisfying the boundary conditions $\mathbf{r}(0) = -1$, $\arg(\mathbf{r}'(0)) = 0$ and $\mathbf{r}(1) = \exp(\mathrm{i}\,\theta)$, $\arg(\mathbf{r}'(1)) = \theta$ with $\kappa(0) = \kappa(1) = 0$, is identified by the coefficients

$$\mathbf{w}_0 \;=\; \sqrt{\frac{30\cos\frac{1}{2}\theta}{6\cos\frac{1}{2}\theta+1}}\,, \quad \mathbf{w}_1 \;=\; 0\,, \quad \mathbf{w}_2 \;=\; \sqrt{\frac{30\cos\frac{1}{2}\theta}{6\cos\frac{1}{2}\theta+1}}\exp(\mathrm{i}\tfrac{1}{2}\theta)\,,$$

and with $\mathbf{p}_0 = (-1, 0)$, $\mathbf{p}_5 = (\cos\theta, \sin\theta)$ the intermediate control points are

$$\mathbf{p}_1 \;=\; \mathbf{p}_2 \;=\; \frac{(-1,0)}{6\cos\frac{1}{2}\theta+1}\,, \quad \mathbf{p}_3 \;=\; \mathbf{p}_4 \;=\; \frac{(\cos\theta,\sin\theta)}{6\cos\frac{1}{2}\theta+1}\,.$$

There are no free parameters, and the quantities (4) are

$$\delta_{\mathrm{m}} \;=\; \frac{(3\cos\frac{1}{2}\theta+8)\,|\sin\frac{1}{2}\theta\,|}{8(6\cos\frac{1}{2}\theta+1)}\,, \quad \kappa_{\mathrm{m}} \;=\; \frac{32\,(6\cos\frac{1}{2}\theta+1)|\tan\frac{1}{2}\theta\,|}{15\,(\cos\frac{1}{2}\theta+1)^2}\,.$$

7.3 G^3 degree 7 PH corner curve

The case $m = 3$ in (15) yields a degree 7 PH corner curve. For a symmetric curve satisfying the G^2 continuity conditions $\arg(\mathbf{r}'(0)) = 0$, $\arg(\mathbf{r}'(1)) = \theta$ and $\kappa(0) = \kappa(1) = 0$, the coefficients must be of the form

$$\mathbf{w}_0 \;=\; p\,, \quad \mathbf{w}_1 \;=\; q\,, \quad \mathbf{w}_2 \;=\; \alpha\, q\exp(\mathrm{i}\tfrac{1}{2}\theta)\,, \quad \mathbf{w}_3 \;=\; \beta\, p\exp(\mathrm{i}\tfrac{1}{2}\theta)\,,$$

where p, q are real values and $\alpha, \beta = \pm 1$. Matching the end points $\mathbf{r}(0) = -1$ and $\mathbf{r}(1) = \exp(\mathrm{i}\,\theta)$ then yields the complex equation

$$\begin{aligned}\frac{1}{7}\Bigg[\,\mathbf{w}_0^2 + \mathbf{w}_0\mathbf{w}_1 + \frac{3\mathbf{w}_1^2+2\mathbf{w}_0\mathbf{w}_2}{5} + \frac{\mathbf{w}_0\mathbf{w}_3+9\mathbf{w}_1\mathbf{w}_2}{10} \\ + \frac{3\mathbf{w}_2^2+2\mathbf{w}_1\mathbf{w}_3}{5} + \mathbf{w}_2\mathbf{w}_3 + \mathbf{w}_3^2\Bigg] \;=\; 1+\cos\theta+\mathrm{i}\sin\theta\,. \qquad (16)\end{aligned}$$

On substituting for $\mathbf{w}_0, \mathbf{w}_1, \mathbf{w}_2, \mathbf{w}_3$, separating real and imaginary parts, and simplifying, we obtain the two real equations

$$(20\cos\tfrac{1}{2}\theta+\alpha)\,p^2 + (10\sec\tfrac{1}{2}\theta+4\alpha+4\beta)\,pq + (12\cos\tfrac{1}{2}\theta+9\beta)\,q^2 = 140\cos\tfrac{1}{2}\theta\,,$$

$$(20\cos\tfrac{1}{2}\theta+\alpha)\,p^2 + (20\,\alpha\beta\cos\tfrac{1}{2}\theta+4\alpha+4\beta)\,pq + (12\cos\tfrac{1}{2}\theta+9\beta)\,q^2 = 140\cos\tfrac{1}{2}\theta\,.$$

These equations are identical if

$$10\sec\tfrac{1}{2}\theta \;=\; 20\,\alpha\beta\cos\tfrac{1}{2}\theta\,, \qquad (17)$$

i.e., if $\alpha\beta = 1$ and $\cos^2 \frac{1}{2}\theta = \frac{1}{2}$, which corresponds to the case of a right–angle corner with $\theta = \pm\frac{1}{2}\pi$. For this particular case there is a one–parameter family of solutions, as described in [6]. When (17) is not satisfied, subtracting the two equations yields the condition

$$(10 \sec \tfrac{1}{2}\theta - 20\,\alpha\beta \cos \tfrac{1}{2}\theta)\, pq \;=\; 0\,,$$

so we must have $p = 0$ or $q = 0$. Discounting the case $p = 0$, since it implies a singular parameterization with $\mathbf{r}'(0) = \mathbf{r}'(1) = 0$, the case $q = 0$ gives

$$\mathbf{w}_0 \;=\; p\,, \quad \mathbf{w}_1 \;=\; \mathbf{w}_2 \;=\; 0\,, \quad \mathbf{w}_3 \;=\; \alpha\, p \exp(\mathrm{i}\tfrac{1}{2}\theta)\,,$$

and to satisfy equation (16) we must then have

$$p^2 \;=\; \frac{140 \cos \frac{1}{2}\theta}{20 \cos \frac{1}{2}\theta + \alpha}\,.$$

We henceforth choose $\alpha = 1$, since $\alpha = -1$ yields solutions with undesirable loops. Thus, we obtain control points $\mathbf{p}_0 = (-1, 0)$, $\mathbf{p}_7 = (\cos\theta, \sin\theta)$ and

$$\mathbf{p}_1 \;=\; \mathbf{p}_2 \;=\; \mathbf{p}_3 \;=\; \frac{(-1, 0)}{20 \cos \frac{1}{2}\theta + 1}\,, \quad \mathbf{p}_4 \;=\; \mathbf{p}_5 \;=\; \mathbf{p}_6 \;=\; \frac{(\cos\theta, \sin\theta)}{20 \cos \frac{1}{2}\theta + 1}\,.$$

Although the above construction imposes only G^2 continuity, the resulting degree 7 PH curves necessarily define a G^3 blend with the incoming/outgoing line segments, since $\mathbf{p}_0, \mathbf{p}_1, \mathbf{p}_2, \mathbf{p}_3$ and $\mathbf{p}_4, \mathbf{p}_5, \mathbf{p}_6, \mathbf{p}_7$ are colinear, and from (3) this implies that $\kappa = \mathrm{d}\kappa/\mathrm{d}s = 0$ at $\xi = 0$ and $\xi = 1$. These G^3 corner curves possess no free parameters, and the quantities (4) are

$$\delta_{\mathrm{m}} \;=\; \frac{(5 \cos \frac{1}{2}\theta + 16)\,|\sin \frac{1}{2}\theta\,|}{16(20 \cos \frac{1}{2}\theta + 1)}\,, \quad \kappa_{\mathrm{m}} \;=\; \frac{96\,(20 \cos \frac{1}{2}\theta + 1)|\tan \frac{1}{2}\theta\,|}{35\,(\cos \frac{1}{2}\theta + 1)^2}\,.$$

Figure 15 shows PH corner curves of degree $3, 5, 7$ and continuity G^1, G^2, G^3 together with their curvature profiles, for the cases $\theta = \frac{1}{4}\pi, \frac{1}{2}\pi, \frac{3}{4}\pi$. Note that increasing the order of continuity causes δ_{m} to diminish, and κ_{m} to increase.

Figure 16 compares the PH corner curves and some optimized "ordinary" polynomial curves with unimodal curvatures[1] for a given geometric continuity and $\theta = \frac{1}{2}\pi$. The G^1 PH cubic and G^1 optimized ordinary cubics appear quite similar. In most instances, the G^2 PH quintic has a smaller deviation δ_{m} and a larger curvature κ_{m} than the G^2 optimized ordinary quartics and quintics, and this difference becomes more pronounced in comparing the G^3 PH septic and the G^3 optimized ordinary sextics.

[1]These correspond to weights (a, b) equal to $(0, 0)$, $(0.1, 0)$, $(0.8, 0.2)$ for cubics; $(0, 0)$, $(0.9, 0.1)$ for quartics; $(0, 0)$, $(0.1, 0)$ for quintics; and $(0, 0)$, $(0.1, 0)$, $(0.3, 0)$ for sextics.

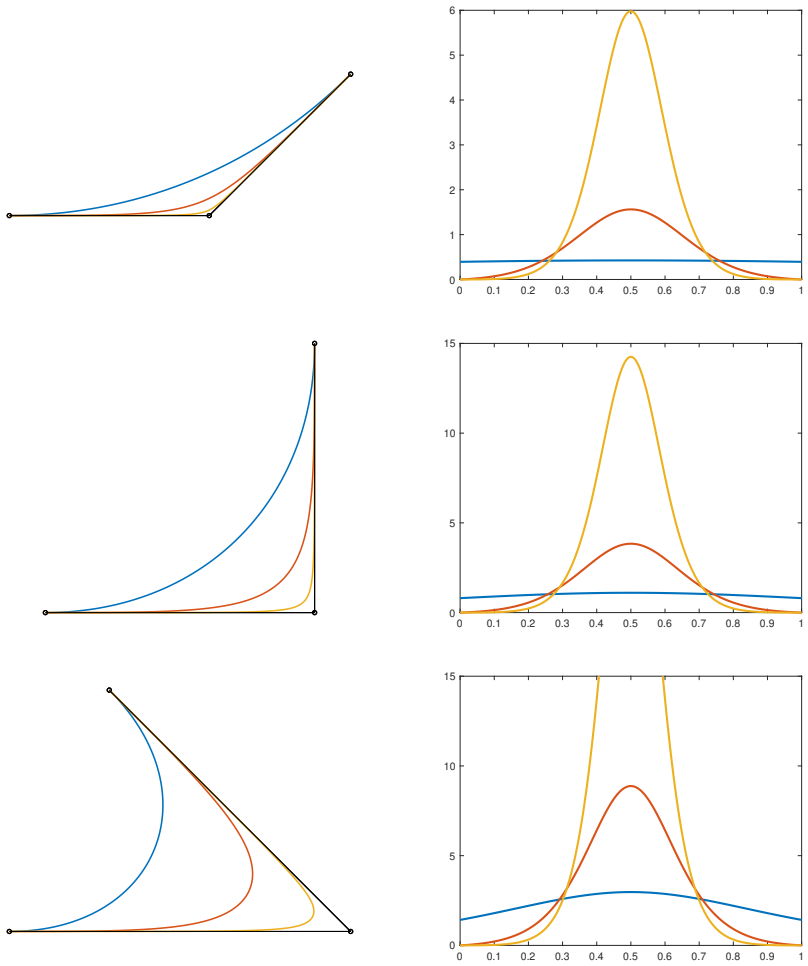

Figure 15: PH corner curves of degree $3, 5, 7$ and continuity G^1, G^2, G^3 with their curvature profiles for angles $\pi/4$ (upper), $\pi/2$ (center), $3\pi/4$ (lower).

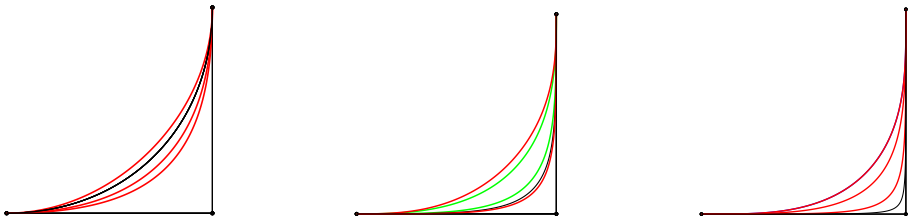

Figure 16: Comparison of the PH and optimized ordinary polynomial corner curves for the angle $\theta = \frac{1}{2}\pi$. Left: G^1 PH cubic (black) with optimized cubics (red). Center: the G^2 PH quintic (black) and optimized quartics (green) and quintics (red). Right: the G^3 PH septic (blue) and optimized sextics (red).

8 Closure

To satisfy various aesthetic or functional requirements, a precise control over the shapes of corner blending curves is often desired, as characterized by the attributes (1)–(3) listed in the Introduction. Polynomial curves of degree ≥ 3 incorporate free parameters to optimize corner shapes, but the formulation of an appropriate optimization objective function requires careful consideration, since the free parameters often conflict in achieving these attributes.

The variation of curvature with arc length, constrained by the imposition of G^k geometric continuity at the end points, is a key measure of corner curve shape quality. However, global curvature variation measures consistent with the boundary conditions do not admit closed–form reduction, and exhibit a complicated dependence on the free parameters. On the other hand, it can be difficult to ensure unimodality of the curvature profile using a local measure, such as the mid–point curvature $\kappa_{\rm m}$, and focusing on the suppression of $\kappa_{\rm m}$ often incurs unacceptably large values of the deviation $\delta_{\rm m}$.

To ensure scale invariance of the corner curves, a dimensionless objective function must be employed in the optimization. However, the product $\kappa_{\rm m}\delta_{\rm m}$ is unsatisfactory, since $\kappa_{\rm m}$ has a stronger dependence on the free parameters than $\delta_{\rm m}$, and this typically yields solutions with singular parameterizations at the end points. To preclude this problem, an objective function was specified as a weighted combination of $\kappa_{\rm m}$ and $\delta_{\rm m}$, normalized by their mean values, together with a normalized term measuring the mean square variation of the parametric speed. The latter term admits closed–form evaluation, and yields solutions that approximate a (scaled) arc–length parameterization.

Experiments based on the objective function (11) and various weights a, b indicate that the best corner shapes are obtained when the parametric speed variation term (10) is dominant. Although this term is not an intrinsic shape measure, it is strongly correlated with the curvature, as seen from the inverse–cubic dependence of $\kappa(\xi)$ on $\sigma(\xi)$ in (3). A constrained optimization problem was also addressed, in which the expression (10) was minimized subject to a specified value of the deviation $\delta_{\rm m}$. Finally, the use of PH curves as corner blends was discussed. These curves have no free parameters, and for higher orders of geometric continuity they are found to yield smaller deviations $\delta_{\rm m}$ and higher curvatures $\kappa_{\rm m}$ than optimized "ordinary" polynomial curves.

The optimization of corner blending curves, so as to exhibit the desirable attributes (1)–(3) defined in the Introduction, is a more subtle problem than might appear at first sight. The proposed objective function (11) is scalable, computationally tractable, and is observed empirically to yield corner curves of excellent shape and near–uniform parametric speed when the term (10) is dominant. The present study does not claim to be exhaustive, and a number of salient points deserve further investigation, including: (i) the identification

of *a priori* constraints on the free parameters that ensure unimodality of the curvature; (ii) the formulation of alternative objective functions that achieve the desired corner curve attributes; and (iii) investigation of the relationship between the order G^k of geometric continuity and the extremum curvature.

References

[1] K. G. Baass (1984), The use of clothoid templates in highway design, *Transport. Forum* **1**, 47–52.

[2] C. A. Ernesto and R. T. Farouki (2012), High–speed cornering by CNC machines under prescribed bounds on axis accelerations and toolpath contour error, *Int. J. Adv. Manufac. Tech.* **58**, 327–338.

[3] R. T. Farouki (1994), The conformal map $z \to z^2$ of the hodograph plane, *Comput. Aided Geom. Design* **11**, 363–390.

[4] R. T. Farouki (1997), Pythagorean–hodograph quintic transition curves of monotone curvature, *Comput. Aided Design* **29**, 601–606.

[5] R. T. Farouki (2008), *Pythagorean–Hodograph Curves: Algebra and Geometry Inseparable*, Springer, Berlin.

[6] R. T. Farouki (2014), Construction of G^2 rounded corners with Pythagorean–hodograph curves, *Comput. Aided Geom. Design* **31**, 127–139.

[7] R. T. Farouki, J. Manjunathaiah, and S. Jee (1998), Design of rational cam profiles with Pythagorean–hodograph curves, *Mech. Mach. Theory* **33**, 669–682.

[8] R. T. Farouki and K. M. Nittler (2016), Efficient high–speed cornering motions based on continuously–variable feedrates I. Real–time interpolator algorithms, *Int. J. Adv. Manufac. Tech.* **87**, 3557–3568.

[9] R. T. Farouki and Y–F. Tsai (2001), Exact Taylor series coefficients for variable–feedrate CNC curve interpolators, *Comput. Aided Design* **33**, 155–165.

[10] G. E. Forsythe, M. A. Malcolm, and C. B. Moler (1976), *Computer Methods for Mathematical Computations*, Prentice Hall, Englewood Cliffs, NJ.

[11] P. E. Gill, W. Murray, M. A. Saunders, and M. H. Wright (1984), Procedures for optimization problems with a mixture of bounds and general linear constraints, *ACM Trans. Math. Software* **10**, 282-298.

[12] P. E. Gill and E. Wong (2012), Sequential quadratic programming methods, in: *Mixed Integer Nonlinear Programming*, (J. Lee and S. Leyffer, eds.) IMA Volumes in Mathematics and its Applications Vol. 154, Springer, New York.

[13] Z. Habib and M. Sakai (2007), G^2 Pythagorean hodograph quintic transition between two circles with shape control, *Comput. Aided Geom. Design* **24**, 252–266.

[14] Z. Habib and M. Sakai (2009), G^2 cubic transition between two circles with shape control, *J. Comput. Appl. Math.* **223**, 133–144.

[15] Z. Habib and M. Sakai (2011), Cubic spiral transition matching G^2 Hermite end conditions, *Numer. Math. Theor. Meth. Appl.* **4**, 525–536.

[16] Z. Habib and M. Sakai (2012), Fairing arc spline and designing by using cubic Bézier spiral segments, *Math. Model. Anal.* **17**, 141–160.

[17] P. Hartman (1957), The highway spiral for combining curves of different radii, *Trans. Amer. Soc. Civil Eng.* **22**, 389–409.

[18] B. M. Imani and J. Jahanpour (2008), High–speed contouring enhanced with PH curves, *Int. J. Adv. Manufac. Tech.* **37**, 747–759.

[19] J. Jahanpour and B. M. Imani (2008), Real–time PH curve CNC interpolators for high speed cornering, *Int. J. Adv. Manufac. Tech.* **39**, 302–316.

[20] D. S. Meek and D. J. Walton (1992), Clothoid spline transition spirals, *Math. Comp.* **59**, 117–133.

[21] K. M. Nittler and R. T. Farouki (2017), Efficient high–speed cornering motions based on continuously–variable feedrates II. Experimental performance analysis, *Int. J. Adv. Manufac. Tech.* **88**, 159–174.

[22] J. Nocedal and S. J. Wright (2006), *Numerical Optimization*, Second Edition, Springer Series in Operations Research, Springer Verlag.

[23] T. Saleem and B. Persaud (2017), Another look at the safety effects of horizontal cuvature on rural two–lane highways, *Accid. Anal. Prev.* **106**, 149–159.

[24] W. H. Schneider, P. T. Savolainen, and D. N. Moore (2010), Effects of horizontal cuvature on single–vehicle motorcylce crashes along rural two–lane highways, *Transportation Research Record*, Issue 2194, 91–98.

[25] B. Sencer, K. Ishikazi, and E. Shamoto (2015), A curvature optimal sharp corner smoothing algorithm for high–speed feed motion generation of NC systems along linear tool paths, *Int. J. Adv. Manufac. Tech.* **76**, 1977–1992.

[26] J. Shi, Q. Z. Bi, Y. H. Wang, and G. Liu (2014), Development of real–time look–ahead methodology based on quintic PH curve with G^2 continuity for high–speed machining, *Appl. Mech. Mater.* **464**, 258–264.

[27] J. Shi, Q. Bi, L. Zhu, and Y. Wang (2015), Corner rounding of linear fixed–axis tool path by dual PH curves blending, *Int. J. Mach. Tools Manuf.* **88**, 223–236.

[28] Z. Šír and B. Jüttler (2005), Constructing acceleration continuous tool paths using Pythagorean hodograph curves, *Mech. Mach. Theory* **40**, 1258–1272.

[29] Z. Šír, E. Wings, and B. Jüttler (2007), Rounding spatial G code tool paths using Pythagorean hodograph curves, *Trans. ASME J. Comput. Inf. Sci, Eng.* **7**, 186–191.

[30] D. J. Walton and D. S. Meek (1996), A planar cubic Bézier spiral, *J. Comput. Appl. Math.* **72**, 85–100.

[31] D. J. Walton and D. S. Meek (1996), A Pythagorean–hodograph quintic spiral, *Comput. Aided Design* **28**, 943–950.

[32] D. J. Walton and D. S. Meek (1998), G^2 curves composed of planar cubic and Pythagorean–hodograph spirals, *Comput. Aided Geom. Design* **15**, 547–566.

[33] D. J. Walton and D. S. Meek (2002), Planar G^2 transition with a fair Pythagorean hodograph quintic curve, *J. Comput. Appl. Math.* **138**, 109–126.

[34] D. J. Walton and D. S. Meek (2004), A generalisation of the Pythagorean hodograph quintic spiral, *J. Comput. Appl. Math.* **172**, 271–287.

[35] D. J. Walton and D. S. Meek (2007), G^2 curve design with a pair of Pythagorean–hodograph quintic spiral segments, *Comput. Aided Geom. Design* **24**, 267–285.

[36] D. J. Walton and D. S. Meek (2009), G^2 blends of linear segments with cubics and Pythagorean–hodograph quintics, *Int. J. Comput. Math.* **86**, 1498–1511.

[37] D. J. Walton and D. S. Meek (2013), Curve design with more general planar Pythagorean–hodograph quintic spiral segments, *Comput. Aided Geom. Design* **30**, 707–721.